Low-Energy Picosecond Magnetic Switching for Synthetic Ferrimagnetic Free Layer Utilizing the Electric-Field-Tuned RKKY Effect

Lei Wang, Xuesong Zhou, Runzi Hao, and Tai Min

Center for Spintronics and Quantum Systems, State Key Laboratory for Mechanical Behavior of Materials, Xi'an Jiaotong University, Xi'an, Shaanxi 710049, China

The precessional switching mechanism has governed the magnetic switching in magnetic tunnel junctions (MTJs) in the sub-nanosecond range, which exponentially increases the switching current density of magnetic random access memory (MRAM). Thus, there needs to be an alternative switching mechanism with much higher energy efficiency to bring down the switching current density significantly and make the MRAM compatible with high-speed L1/2—static random access memory (SRAM) at sub-nanosecond range. Using the recent discovered external electric field (*E*-field) tunable Ruderman–Kittel–Kasuya–Yosida (RKKY) phenomena in a synthetic ferrimagnet (E-SFi), we propose a totally different *Chrysanthemum*-like switching mechanism to realize a low-energy picosecond writing MRAM design, which breaks the precessional switching mechanism at picosecond region. And our results show that the critical switching current density can be significantly reduced by one order of magnitude compared to that of a conventional MTJ design down to 100 ps. In addition, we study the robustness of the asynchronous conditions between the charge current pulse and the *E*-field pulse for its practical applications.

***Index Terms*—Low switching current, magnetic random access memory (MRAM), picosecond magnetic switching, Ruderman–Kittel–Kasuya–Yosida (RKKY) interaction, synthetic ferrimagnet.**

I. Introduction

BECAUSE of its nonvolatility, high speed, and high density, magnetic random access memory (MRAM) has received extensive attention in both research [1]–[6] and industry [7]–[13]. The core functional element in MRAM is the magnetic tunnel junctions (MTJs) based on two magnetic layers sandwiching a tunnel barrier, in which a high tunnel magnetoresistance ratio (TMR) [14]–[17] is used to read the data bits and a spin/polarized-charge current is used to write (spin orbit torque [4], [6], [12], [13] or spin transfer torque (STT) [18], [19]). However, when the writing process becomes static random access memory (SRAM) like (<1 ns), the critical charge current for switching of MRAM increases exponentially based on precessional switching mechanics [20], [21], which can even break down the tunnel barrier in the MTJs [22]. Therefore, the current MRAM designs still have not been competitive with the high-speed L1/2-SRAM. In this sense, reducing the switching current density at sub-nanosecond region has been a continuous challenge for long time.

Many efforts have been carried out to reduce the high switch current generally required of current MRAM technology, e.g., the voltage-controlled magnetic anisotropy (VCMA) approach [23]–[35], in which the magnetic anisotropy of free layer can be changed from perpendicular to in plane by an applied external electric field, which changes the magnetization from out of plane to in plane and assists the magnetic switching to reduce the required switching current. Recently, it had been proven that the ground state of a synthetic antiferromagnet (e.g., CoFeB/Ru/CoFeB or $(Pt/Co)_2/Ru/(Co/Pt)_2$) can be changed from an antiferromagnetic (AFM) coupling state to a ferromagnetic (FM) coupling state only by a relative small external electric field (*E*-field) [36]–[39] by tuning the sign of the Ruderman–Kittel–Kasuya–Yosida (RKKY) interaction [40]–[43]. In this case, an initial AFM coupling state can be changed to FM coupling state by the electric field; the magnetizations of the two magnetic layers of the synthetic AFM structure is aligned, in which one magnetic layer has been 180° reversed. Thus, the *E*-field-tuned RKKY interaction impacts the magnetizations of the free layer differently from the VCMA using an AFM-FM phase transition instead of changing of magnetic anisotropy. This novel *E*-field-tuned RKKY effect had inspired us to design a new MTJ structure by replacing the conventional FM-free layer with an E-SFi-free layer design, which using the *E*-field-tuned AFM-to-FM phase transition to assist magnetic switching [44]. Here, we studied the sub-nanosecond switching behavior of the E-SFi design with various current/*E*-field pulse periods, using a conventional FM-free layer with the same thermal stability as a benchmark. We found that the switching mechanism of the E-SFi MRAM design is non-precessional. The writing energy and critical switching current can be significantly reduced by the *E*-field-tuned AFM-FM phase transition. With detailed study of the dynamics of the spins, we observed a complex *Chrysanthemum*-like texture during the switching process, which breaks the coherent precessional switching behavior for conventional FM-free layer design in this time scale. Moreover, the robustness of asynchronous charge current and *E*-field pulse was studied for practical applications.

Manuscript received February 25, 2021; revised May 19, 2021; accepted June 22, 2021. Date of publication June 24, 2021; date of current version July 20, 2021. Corresponding author: T. Min (e-mail: tai.min@xjtu.edu.cn).

Color versions of one or more figures in this article are available at https://doi.org/10.1109/TMAG.2021.3092166.

Digital Object Identifier 10.1109/TMAG.2021.3092166

0018-9464 © 2021 IEEE. Personal use is permitted, but republication/redistribution requires IEEE permission.
See https://www.ieee.org/publications/rights/index.html for more information.

Authorized licensed use limited to: Xian Jiaotong University. Downloaded on August 05,2021 at 01:44:58 UTC from IEEE Xplore. Restrictions apply.

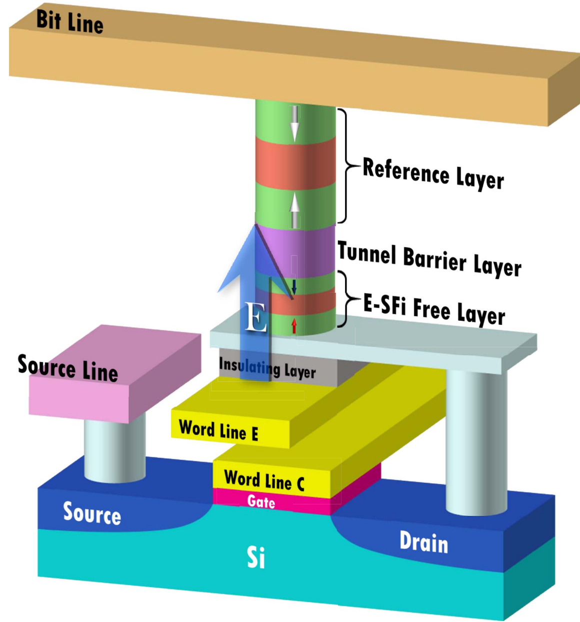

Fig. 1. Sketch model of the new STT-MRAM, with E-SFi layers as a magnetic free layer. An extra electrode (Word Line E) is introduced to generate the E-field, while the Word Line C is for generating charge current. An insulating layer is used to decouple E-field and MTJ.

II. Model and Method

The E-SFi-free layer design to replace the conventional FM-free layer can be used for various writing methods such as the STT or spin orbit torque. In this article, we focused on investigating the switching behavior of the E-SFi structure using STT as an example. The proposed E-SFi MRAM design is shown in Fig. 1, where an extra electrode (Word Line E) is introduced to generate a small E-field for the AFM-FM phase transition in E-SFi [36]. An insulating layer is inserted between Word Line E and Word Line C to prevent the coupling between the E-field and charge current. The E-field will not affect the injected charge current from Word Line C. Here, we should notice that this is not the only way to generate E-field: one may alternatively use an inserting layer of ferroelectric materials instead, or other reliable methods. And as the AFM-FM phase transition in the E-SFi is independent to the direction of the E-field [36], one can feel free to generate external E-field in many ways. The sketch model of the MTJ in our proposed E-SFi-based MRAM is also shown inside Fig. 1, consisting of a E-SFi-free layer and a reference layer sandwiching a tunnel barrier (e.g., MgO or Al_2O_3). In this case, the storage bits are determined by the order (parallel or anti-parallel) between the magnetization of the two magnetic layers near the tunnel barrier layer, because the tunneling magneto resistance (TMR) in the whole device is dominated by the magnetic layer close to the tunnel barrier. And because the direction of the magnetization in the reference layer are fixed in both reading and writing process, the information of the E-SFi-free layer is much more important in our study. Thus, we only use the E-SFi-free layer to do our simulations with injecting polarized charge currents to reproduce the STT effect.

To investigate the spin dynamics of the E-SFi, micromagnetic simulations are carried out using the Object-Oriented Micromagnetic Framework [45] code, and we use the similar CoFeB/Ru/CoFeB structure from the [36] as the E-SFi for the numerical calculations. In detail, we set up a nanopillar with diameter $d = 50$ nm, and thickness $t = 2.8$ nm, which consists of two CoFeB layers ($t_{\text{bottom}} = 1.2$ nm and $t_{\text{top}} = 0.8$ nm for the bottom and top layers, respectively) and one Ru ($t_{\text{Ru}} = 0.8$ nm) layer. The E-SFi is discretized into a lattice of rectangular cells with size of $2\text{ nm} \times 2\text{ nm} \times 0.4$ nm.

As we know, the dynamics of the spins are governed by the Landau–Lifshitz–Gilbert–Slonczewski (LLGS) [46]–[49] equation, which reads

$$\frac{d\mathbf{m}}{d\tau} = -\gamma\,\mathbf{m} \times \mathbf{H}_{\text{eff}} + \alpha\mathbf{m} \times \frac{d\mathbf{m}}{d\tau} + \Gamma_{\text{STT}} \tag{1}$$

where $\mathbf{m}$ is the direction of the magnetization, τ the time, γ the gyromagnetic ratio, $\mathbf{H}_{\text{eff}}$ the effective magnetic field, and the damping constant $\alpha = 0.01$ for used CoFeB [50], [51]. In addition, the STT Γ_{STT} generally comes from the injecting polarized charge current, written as

$$\Gamma_{\text{STT}} = \gamma\beta\epsilon(\mathbf{m} \times \mathbf{m}_p \times \mathbf{m}) - \gamma\beta\epsilon'\mathbf{m} \times \mathbf{m}_p \tag{2}$$

with $\beta = (\hbar \text{J}/(|e|\mu_0 t M_s))$, where $\hbar$ is the reduced Planck constant, J the charge current density, e the electron charge, μ_0 the vacuum permeability, t the thickness of E-SFi-free layer, and the saturation magnetization of magnetic CoFeB layer in the E-SFi-free layer $M_s = 1.26 \times 10^6$ A/m [52], and

$$\epsilon = \frac{P\Lambda^2}{(\Lambda^2 + 1) + (\Lambda^2 - 1)(\mathbf{m} \cdot \mathbf{m}_p)} \tag{3}$$

where $P = 0.93$ is the polarization of the charge current with polarized direction $\mathbf{m}_p$, and we use $\Lambda = 1$ to remove the dependence of ϵ on $\mathbf{m} \cdot \mathbf{m}_p$ to make the STT isotropic. And as the ratio of the field-like STT to Slonczewski STT ϵ'/ϵ in MgO-based MTJs varies from 0.1 to 0.3 [53]–[56], we set the secondary spin transfer term $\epsilon' = 0.07$ to have an ordinary ratio $\epsilon'/\epsilon = 0.15$.

Besides the general parameters of the materials in the E-SFi as shown above, the total energy of the E-SFi-free layer includes several parts, e.g., the Heisenberg exchange energy E_{ex} with the Heisenberg exchange coefficients $A = 3 \times 10^{-13}$ J/cm from CoFeB [57], [58], the demagnetizing energy E_{de}, the anisotropy energy $E_{\text{an}} = KV$ with the effective magnetic anisotropy constants K and volume V of the E-SFi. However, we know that the magnetic anisotropy in MgO-based MTJs mainly comes from the interface, thus we only use a typical interface magnetic anisotropy constant in our calculations, which are $K^i_{\text{bott}} = 1.44 \times 10^{-7}$ J/cm^2 and $K^i_{\text{top}} = 0.96 \times 10^{-7}$ J/cm^2 [52] for bottom layer and top layer of the E-SFi-free layer, respectively. Here, the different interface magnetic anisotropy constants are intentionally chosen to make the bottom layer of the E-SFi more stable than the top layer of the E-SFi to store data bits. In this design, the thermal stability (Δ) of the E-SFi can be obtained using the

Authorized licensed use limited to: Xian Jiaotong University. Downloaded on August 05,2021 at 01:44:58 UTC from IEEE Xplore. Restrictions apply.

well-known formula [52], [59]

$$\Delta = \frac{K^i_{\text{bott}}/t_{\text{bott}} - \mu_0 M_s^2/2}{k_B \mathcal{T}} V_{\text{bott}} + \frac{K^i_{\text{top}}/t_{\text{top}} - \mu_0 M_s^2/2}{k_B \mathcal{T}} V_{\text{top}} \quad (4)$$

where V_{bott} and V_{top} are the volume of the bottom layer and top layer of the E-SFi, respectively, k_B is the Boltzmann's constant, and $\mathcal{T}$ is the temperature. Therefore, we have $\Delta \simeq 199$ at room temperature $\mathcal{T} = 300$ K, which is much more than $\Delta = 40 \sim 75$ needed for ten years retention of the data [60]–[63].

In addition, for CoFeB/Ru/CoFeB structure, it has been demonstrated that the AFM coupling state can change to FM coupling state with a small estimated electric field by applying a small voltage $\phi_0 \simeq 2$ V [36]. Following Thomas–Fermi screening theory, the potential along the z-axis (perpendicular to the interfaces) is $\phi(z) = \phi_0[e^{-z/L_D} - e^{-(d-z)/L_D}]$, where ϕ_0 is the gating voltage on one side of the thin film, L_D is the Debye length, and d is the thickness of the thin film. And the corresponding E-field will be $\mathbf{E}(z) = -\partial\phi(z)/\partial z$. With the parameters from [36], in which we have the structure of the sample as CoFeB (1.5 nm)/Ru (1.0 nm)/ CoFeB (1.5 nm), therefore the thickness $d = 4$ nm. However, as we do not find the experimental L_D of the CoFeB and Ru, we use the Debye length of an Au nanoparticle [64] with a value of $L_D = 1$ nm as a typical number for both CoFeB and Ru, and then the E-filed around the interfaces will be $\mathbf{E} \simeq 0.61$ V/nm, which is quite close to that from a linear chemical potential approximation [36], where the E-field is $\mathbf{E} = \phi_0/d = 0.5$ V/nm. In our approach, this E-field-controlled AFM-FM phase transition can be modeled by adding an extra energy term in the calculations and reads

$$E_{RKKY} = \int_{i \in S} E_i \, dV \quad (5)$$

where

$$E_i = \sum_{j \in S} \frac{\sigma(1 - \mathbf{m}_i \cdot \mathbf{m}_j)}{\delta_{ij}} \quad (6)$$

is the density of the RKKY exchange energy of surface cell i relative to all matching surface cells j around the interfaces (S), δ_{ij} is the corresponding discretization cell size, and σ represents the RKKY coefficient between the two magnetic layers. In this sense, the AFM to FM phase transition by the electric field in E-SFi can be governed by changing the sign of σ.

III. Results and Analysis

In this work, we mainly investigated the magnetic switching of the E-SFi, in which the critical switching current density J_{sw} and charge current pulse width T_J are the most important parameters. The inset of Fig. 2 shows a sketch of the charge current pulse and E-field pulse for the E-SFi, and we fixed the E-field pulse width $T_E = 0.5$ T$_J$ and put the E-field pulse in the middle of the charge current pulse for this case. Additionally, we marked four typical time points $\tau_{i,i\in\{1,2,3,4\}}$,

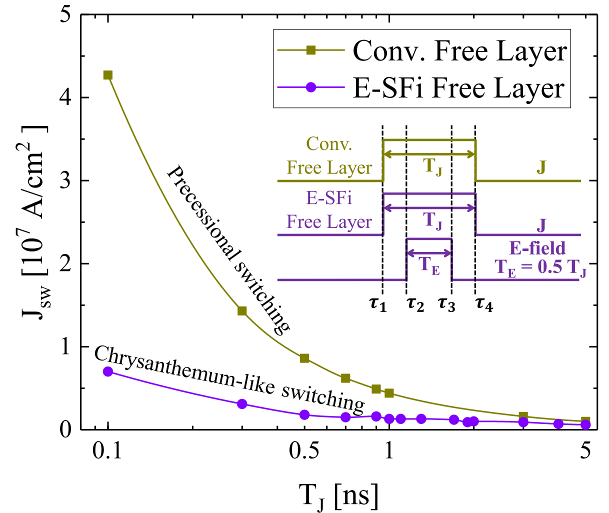

Fig. 2. Critical switching current density J_{sw} versus the current pulse width T_J for the conventional free layer and the E-SFi-free layer. The inset shows the sketch of the applied charge current pulse J with pulse width T_J for both the conventional free layer and E-SFi-free layer, and the corresponding external E-field pulse with pulse width T$_E$ = 0.5 T$_J$ for the E-SFi-free layer only.

where the charge current and E-field pulse are turned on and off, respectively. For comparison, a conventional FM-free layer switched only by a polarized current was calculated with a similar thermal stability factor $\Delta \simeq 199$.

The calculated J$_{\text{sw}}$ versus T_J is plotted in Fig. 2 for both the conventional FM and E-SFi-free layers. The J$_{\text{sw}}$ for the conventional FM-free layer increases exponentially, which is determined by precessional switching mechanics [20], as expected from a previous publication [21]. However, for the E-SFi, the J$_{\text{sw}}$ decreases by almost one order of magnitude at $T_J = 0.1$ ns, and still ~3.6 times smaller at $T_J = 0.75$ ns. And according to [22], the writing voltage increases exponentially for conventional STT-MRAM and increases three times from breakdown-safe [65] ~0.5 V at $T_J = 10$ ns to ~1.5 V at $T_J = 0.75$ ns, which is close to/more than the breakdown voltage (1.26–1.40 V at RA = 5 $\Omega\mu$m^2) of the tunnel barrier (~1 nm) of the MTJs from [66]. In this sense, the ~3.6 times reduction of the J$_{\text{sw}}$ at $T_J = 0.75$ ns for E-SFi-free layer can make the writing voltage back to a breakdown-safe value (~0.42 V), therefore the E-SFi MRAM could work safely at sub-1-ns region, which makes it compatible with the L1/2-SRAM at the sub-7-nm technology node [8], [67].

To understand the underlying physical origin of the E-field-assisted ultrafast switching in the E-SFi, we studied the time-dependent multiple energy terms as shown in Fig. 3(a). We can see that, the RKKY interaction energy (E_{RKKY}) exhibits a sharp jump when the E-field is turned on (τ_2), ahead of the Heisenberg exchange energy (E_{ex}) and dominating the sharp increase of the total energy (E_{tot}). It is well known that, in conventional MRAM, there is an energy barrier between the two spin states, up and down, which determines how much energy is needed to switch the magnetization. In which, only the applied polarized charge current will supply enough angular momentum to overcome the energy barrier with a precessional switching behavior [20], [21]. However, for the

Authorized licensed use limited to: Xian Jiaotong University. Downloaded on August 05,2021 at 01:44:58 UTC from IEEE Xplore. Restrictions apply.

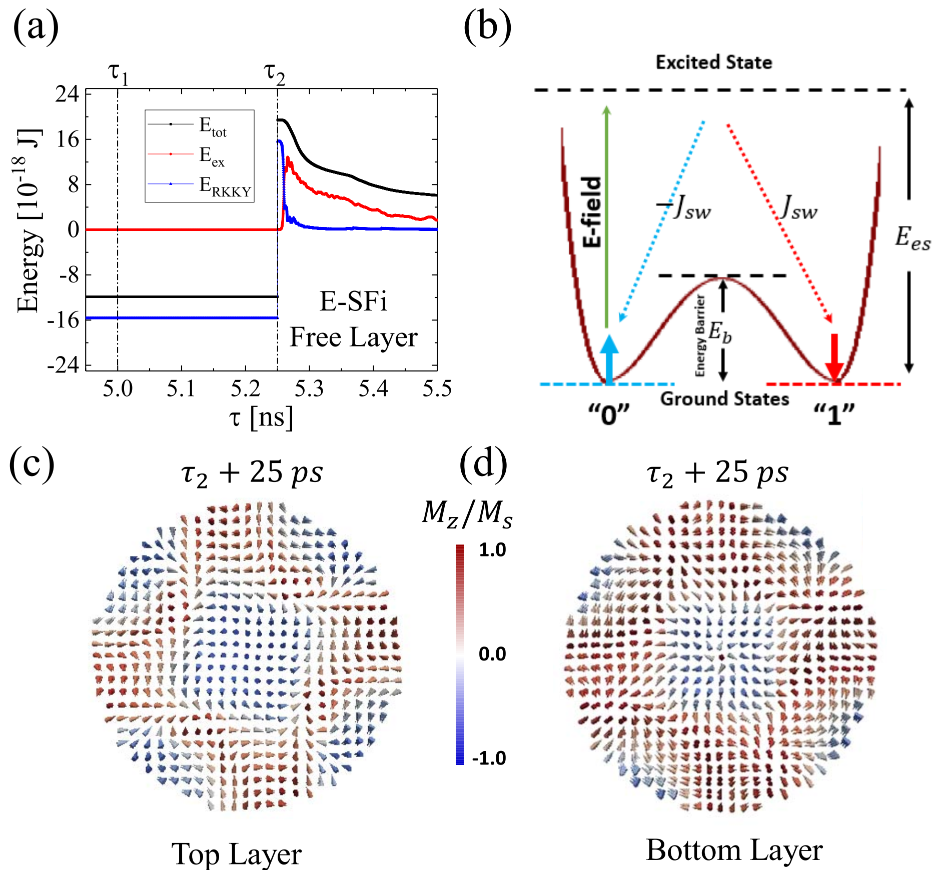

Fig. 3. (a) Calculated energies versus time (τ) for the E-SFi-free layer with $T_J = 1$ ns, where E_{tot} is the total energy, E_{ex} is the Heisenberg exchange energy, E_{RKKY} is the RKKY interaction energy. (b) Toy model of the ultrafast switching mechanism of the E-SFi under the applied E-field. (c) and (d) are the corresponding spin textures of the top and bottom layers of the E-SFi at 25 ps after turn-on time of the E-field (τ_2).

E-SFi, when the E-field is on, the sign of the RKKY interaction changes, and E_{tot} increases suddenly by a value of twice of the E_{RKKY} without E-field according to (6), and verified by the calculations as shown in Fig. 3(a). This extra energy excites the magnetization from one ground state to an excited state (with energy level E_{es}) that is much larger than the energy barrier E_b of a conventional FM-free layer with identical Δ. When it comes back to the ground states (spin up or down), only a small polarized charge current is needed to guide the magnetization to the expected state using its current direction. In this sense, the direction-guiding J_{sw} in the E-SFi can be significantly smaller than the energy-barrier-overcoming J_{sw} in the conventional FM-free layer. This E-SFi switching mechanism can be represented by a toy model as shown in Fig. 3(b). We also investigated the detailed spin textures of the E-SFi during switching, we observed a complex *Chrysanthemum*-like spin structure only 25 ps after turning on the E-field as shown in Fig. 3(c) and (d). The *Chrysanthemum*-like structures are very different from the precessional switching mode, in which the spins are uniform at all times because of the Heisenberg exchange interaction. This is the underlying physical origin of the E-SFi switching that does not obey the precessional switching mechanism.

Thus, the whole switching process of the E-SFi can be illustrated as shown in Fig. 4. It can be seen that the E-SFi layer has an initial AFM state with spin up in the bottom layer and spin down in the top layer. And the AFM state keeps unchanged until applying the external E-field at τ_2. Then, only 25 ps after turning on the E-field, both the spin textures of the bottom layer and top layer are destroyed and become *Chrysanthemum*-like. From τ_2 to τ_3, the spins start to evolve to FM state under the control of the E-field-induced AFM-FM phase transition. Moreover, with the help of the polarized charge current, most of the spins are forced to point to $-z$-direction (spin down, blue color). Therefore, when turning off the E-field at τ_3, the spins will evolve to AFM state again but with spin down in bottom layer and spin up in top layer. In this sense, all the spins inside the E-SFi are switched at τ_5 as shown in Fig. 4.

In addition, we studied the asynchronous conditions between the charge current pulse and the E-field pulse. First, we changed the turn-off time of the E-field τ_3 behind the turn-off time of the charge current τ_4, as shown in the inset of Fig. 5(a). The corresponding results of the J_{sw} versus E-field lagging time $\Delta T_{\text{lag}} = \tau_3 - \tau_4$ for various current pulse width T_J are plotted in Fig. 5(a), in which we found J_{sw} is insensitive to the ΔT_{lag} (up to 10 ns) for various charge current pulsewidths T_J ($0.1 \sim 5.0$ ns). These results can also be understood within the framework of the previous toy model, when E-field is on at τ_2, the ground state of the E-SFi jump to a high energy

Authorized licensed use limited to: Xian Jiaotong University. Downloaded on August 05,2021 at 01:44:58 UTC from IEEE Xplore. Restrictions apply.

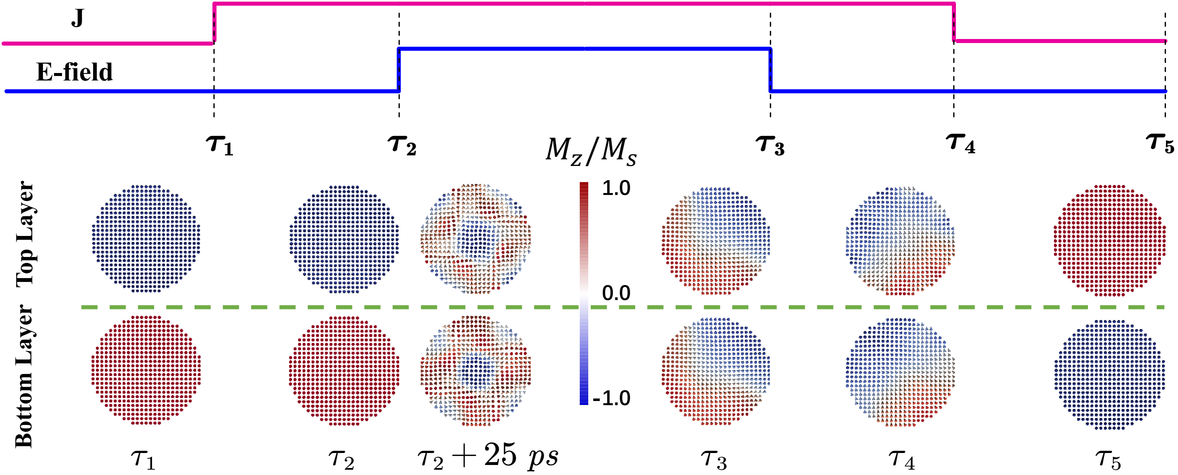

Fig. 4. Whole time-evolution process of the spins in both the top layer and bottom layer of the E-SFi with $T_J = 1$ ns, where $\tau_{i,i\in\{1,2,3,4,5\}}$ labels the corresponding time points of the current and E-field pulses.

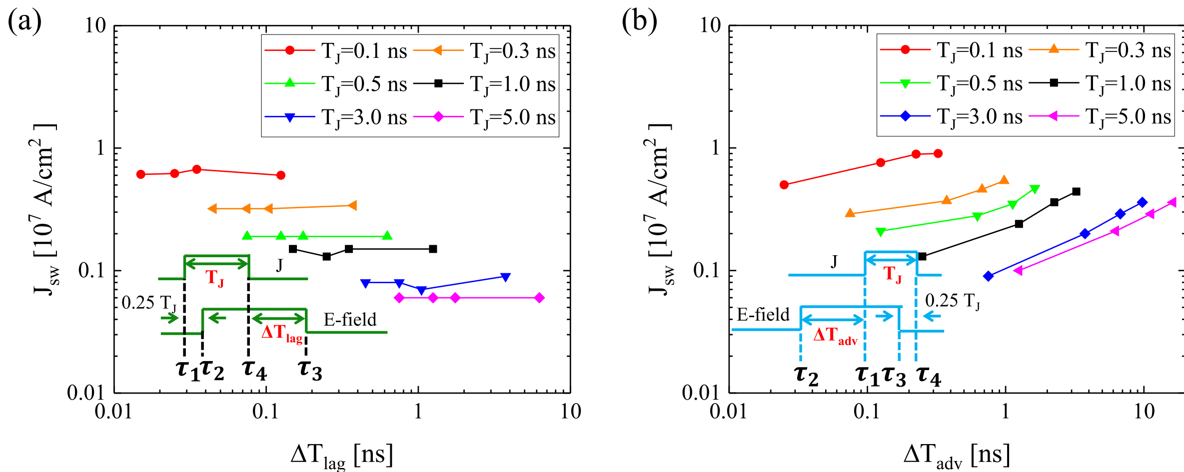

Fig. 5. Critical switching current density J_{sw} with asynchronous charge current and E-field pulses, where the insets are the corresponding sketches of the detailed parameters of the current and E-field pulses; e.g., (a) and (b) plot J_{sw} versus the lagging time and advance time between the E-field and the charge current for various T_J.

level (E_{es}). Within a short time $\Delta\tau$ (e.g., ~25 ps in Fig. 3 with $T_J = 1.0$ ns) after τ_2, the magnetization pattern of the E-SFi changes from uniform to a complex *chrysanthemum*-like texture as shown in Fig. 3(c) and (d). The evolution of this texture is governed by the small polarized charge current J_{sw}, but not strongly dependent on the remaining E-field, as shown by the rapid drop of the E_{RKKY} around τ_2 in Fig. 3(a). Thus, the low-energy ultrafast switching by the small J_{sw} is robust when the pulse width of the E-field is longer than its corresponding $\Delta\tau$.

Similarly, as shown in the inset of Fig. 5(b), we changed the turn-on time of the E-field τ_2 ahead of the turn-on time of the charge current τ_1, and define $\Delta T_{adv} = \tau_1 - \tau_2$. The calculated results are plotted in Fig. 5(b), in which we found J_{sw} increases with increasing ΔT_{adv}. This is because when the E-field turns on ahead of the charge current, the E-SFi will change from an AFM coupling state to *Chrysanthemum*-like state suddenly and will start to evolve to an FM coupling state before the polarized charge current provides any contribution. For example, for a long enough T_{adv}, the E-SFi will evolve to a FM coupling state completely before the turn-on time of the polarized charge current, making it identical to the conventional FM-free layer design. Then the energy barrier will be overcome by the polarized charge current only. For MRAM to be a candidate to replace L1/2–SRAM at the sub-7 nm technology node, it is essential to have a small and breakdown-safe critical switching current at sub-nanosecond range. Our study shows that this goal can be achieved with this novel E-SFi design by turning on the E-field pulse simultaneously or after the polarized charge current and the turn-off time of the E-field is not critical.

The robustness of the switching in the E-SFi is very important for practical applications. Thus, we studied its dependence on various parameters as shown in Fig. 6, with which we concluded that the switching current of the E-SFi-free layer design is quite robust against the thermal stability, disorder, and turn on time of the charge and E-field pulses. This can be also understood by the toy model in Fig. 3, as the

Authorized licensed use limited to: Xian Jiaotong University. Downloaded on August 05,2021 at 01:44:58 UTC from IEEE Xplore. Restrictions apply.

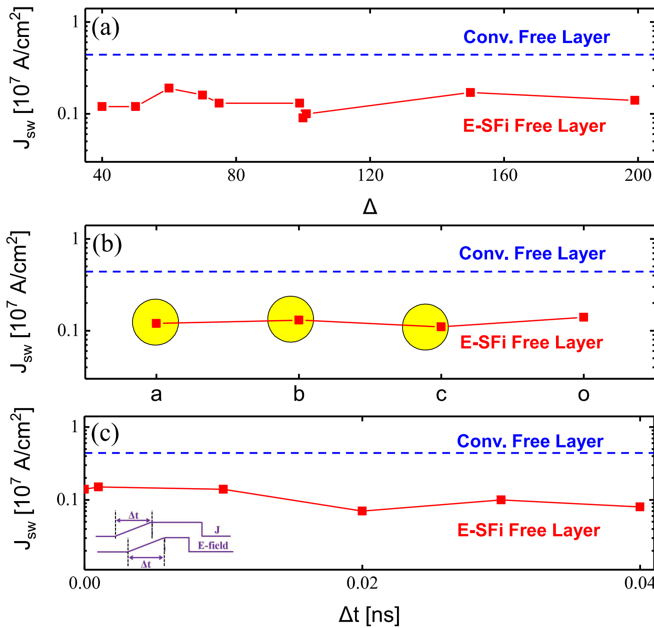

Fig. 6. Robustness of the switching current against various parameters at $T_J = 1$ ns. (a) J_{sw} versus thermal stability Δ by multiplying the same factor to both K^i_{bott} and K^i_{top}. (b) J_{sw} versus disorder, where we remove the magnetic moment of one cell with the size of 2 nm $\times$ 2 nm $\times$ 0.4 nm to simulate a nonmagnetic disorder for three typical locations: center, middle, and edge, which are sketched by the yellow circulars and the position of the data points. "o" is for the results without disorder. (c) J_{sw} versus turn on time Δt for the current and E-field pulses, the inset map shows the sketch of the applied charge and E-field pulses. The blue dash lines represent the switching current of the conventional FM-free layer at $T_J = 1$ ns from Fig. 2 for comparison.

E-field-induced ground state excitation is independent of the above parameters, and the high energy-level E_{es} of the excited state makes the corresponding finite disturbance irreverent. Thus, we have strong confidence that our design has a great possibility of implementation in the future.

IV. Conclusion

In summary, the magnetic switching dynamics in a novel E-SFi-free layer design is investigated by micromagnetic simulations in this article. The critical switching current density can be reduced by one order of magnitude at 100 ps, making it potential candidate to replace L1/2-SRAM. To understand this ultrafast low-energy magnetic switching, the energy evolution has been studied and a toy model has been proposed. In this toy model the small E-field is used to excite the magnetic state of E-SFi from a ground state to an energy level E_{es} that is much higher than the conventional energy barrier E_b, and the small polarized charge current is only needed to guide the magnetization to the expected state.

For the possible practical use of the E-SFi MRAMs, we investigated the effects of asynchronous charge current and E-field pulses. We found that, to have ultralow critical switching current, the E-field should not be applied ahead of the polarized charge current. Fortunately, the small critical switching current density is quite robust when the turn-off time of the E-field pulse is lagged the turn-off time of charge current pulse (within 10 ns in our calculations). Thus, the best strategy for applying the E-field is to turn on the E-field slightly later than the charge current pulse and to maintain the E-field as long as desired.

Acknowledgment

This work was supported in part by the National Key Research and Development Program of China under Grant 2018YFB0407600, Grant 2017YFA0206202, and Grant 2016YFA0300702; in part by the National Natural Science Foundation of China under Grant 11804266; and in part by the Shaanxi Province Science and Technology Innovation Project under Grant 2015ZS-02 and Grant 2019TSLGY08-04.

References

[1] M. Gajek *et al.*, "Spin torque switching of 20 nm magnetic tunnel junctions with perpendicular anisotropy," *Appl. Phys. Lett.*, vol. 100, no. 13, Mar. 2012, Art. no. 132408.

[2] A. V. Khvalkovskiy *et al.*, "Basic principles of STT-MRAM cell operation in memory arrays," *J. Phys. D, Appl. Phys.*, vol. 46, no. 7, Feb. 2013, Art. no. 074001.

[3] T. Kawahara, K. Ito, R. Takemura, and H. Ohno, "Spin-transfer torque RAM technology: Review and prospect," *Microelectron. Rel.*, vol. 52, pp. 613–627, Apr. 2012.

[4] L. Liu, C.-F. Pai, Y. Li, H. W. Tseng, D. C. Ralph, and R. A. Buhrman, "Spin-torque switching with the giant spin Hall effect of tantalum," *Science*, vol. 336, no. 6081, p. 555, 2012.

[5] X. Zhang *et al.*, "Electrical control over perpendicular magnetization switching driven by spin-orbit torques," *Phys. Rev. B, Condens. Matter*, vol. 94, no. 17, Nov. 2016, Art. no. 174434.

[6] J. Han, A. Richardella, S. A. Siddiqui, J. Finley, N. Samarth, and L. Liu, "Room-temperature spin-orbit torque switching induced by a topological insulator," *Phys. Rev. Lett.*, vol. 119, no. 7, Aug. 2017, Art. no. 077702.

[7] W. Kim *et al.*, "Extended scalability of perpendicular STT-MRAM towards sub-20 nm MTJ node," in *IEDM Tech. Dig.*, Dec. 2011, pp. 24.1.1–24.1.4.

[8] J. M. Slaughter *et al.*, "High density ST-MRAM technology (Invited)," in *IEDM Tech. Dig.*, Dec. 2012, pp. 29.3.1–29.3.4.

[9] S. Tehrani, "Status and outlook of MRAM memory technology (Invited)," in *IEDM Tech. Dig.*, 2006, pp. 1–4.

[10] T. Min *et al.*, "A study of write margin of spin torque transfer magnetic random access memory technology," *IEEE Trans. Magn.*, vol. 46, no. 6, pp. 2322–2327, Jun. 2010.

[11] T. Min *et al.*, "Interconnects scaling challenge for sub-20 nm spin torque transfer magnetic random access memory technology," in *Proc. IEEE Int. Interconnect Technol. Conf.*, May 2014, pp. 341–344.

[12] Q. Shao *et al.*, "Large room temperature charge-to-spin conversion efficiency in topological insulator/CoFeB bilayers," in *Proc. 76th Device Res. Conf. (DRC)*, Jun. 2018, pp. 1–2.

[13] Q. Shao *et al.*, "Room temperature highly efficient topological insulator/Mo/CoFeB spin-orbit torque memory with perpendicular magnetic anisotropy," in *IEDM Tech. Dig.*, Dec. 2018, p. 36.

[14] W. H. Butler, X.-G. Zhang, T. C. Schulthess, and J. M. MacLaren, "Spin-dependent tunneling conductance of Fe|MgO|Fe sandwiches," *Phys. Rev. B, Condens. Matter*, vol. 63, Jan. 2001, Art. no. 054416.

[15] J. Mathon and A. Umerski, "Theory of tunneling magnetoresistance of an epitaxial Fe/MgO/Fe(001) junction," *Phys. Rev. B, Condens. Matter*, vol. 63, no. 22, May 2001, Art. no. 220403.

[16] S. S. P. Parkin *et al.*, "Giant tunnelling magnetoresistance at room temperature with MgO (100) tunnel barriers," *Nature Mater.*, vol. 3, no. 12, pp. 862–867, Dec. 2004.

[17] M. Wang *et al.*, "Current-induced magnetization switching in atom-thick tungsten engineered perpendicular magnetic tunnel junctions with large tunnel magnetoresistance," *Nature Commun.*, vol. 9, no. 1, p. 671, Feb. 2018.

[18] J. C. Slonczewski, "Current-driven excitation of magnetic multilayers," *J. Magn. Magn. Mater.*, vol. 159, nos. 1–2, pp. L1–L7, Jun. 1996.

[19] L. Berger, "Emission of spin waves by a magnetic multilayer traversed by a current," *Phys. Rev. B, Condens. Matter*, vol. 54, no. 13, pp. 9353–9358, Oct. 1996.

[20] J. Z. Sun, "Spin-current interaction with a monodomain magnetic body: A model study," *Phys. Rev. B, Condens. Matter*, vol. 62, no. 1, pp. 570–578, Jul. 2000.

Authorized licensed use limited to: Xian Jiaotong University. Downloaded on August 05,2021 at 01:44:58 UTC from IEEE Xplore. Restrictions apply.

[21] Z. Diao *et al.*, “Spin-transfer torque switching in magnetic tunnel junctions and spin-transfer torque random access memory,” *J. Phys., Condens. Matter*, vol. 19, no. 16, Apr. 2007, Art. no. 165209.

[22] G. Jan *et al.*, “Achieving sub-ns switching of STT-MRAM for future embedded LLC applications through improvement of nucleation and propagation switching mechanisms,” in *Proc. IEEE Symp. VLSI Technol.*, Jun. 2016, pp. 1–2.

[23] T. Maruyama *et al.*, “Large voltage-induced magnetic anisotropy change in a few atomic layers of iron,” *Nature Nanotechnol.*, vol. 4, no. 3, pp. 158–161, Mar. 2009.

[24] W.-G. Wang, M. Li, S. Hageman, and C. L. Chien, “Electric-field-assisted switching in magnetic tunnel junctions,” *Nature Mater.*, vol. 11, no. 1, pp. 64–68, Jan. 2012.

[25] P. K. Amiri and K. L. Wang, “Voltage-controlled magnetic anisotropy in spintronic devices,” *SPIN*, vol. 2, no. 3, Sep. 2012, Art. no. 1240002.

[26] W. Kang, Y. Ran, Y. Zhang, W. Lv, and W. Zhao, “Modeling and exploration of the voltage-controlled magnetic anisotropy effect for the next-generation low-power and high-speed MRAM applications,” *IEEE Trans. Nanotechnol.*, vol. 16, no. 3, pp. 387–395, May 2017.

[27] K. L. Wang, H. Lee, and P. K. Amiri, “Magnetoelectric random access memory-based circuit design by using voltage-controlled magnetic anisotropy in magnetic tunnel junctions,” *IEEE Trans. Nanotechnol.*, vol. 14, no. 6, pp. 992–997, Nov. 2015.

[28] P. Khalili and K. Wang, “Electric-field-controlled MRAM based on voltage control of magnetic anisotropy (VCMA): Recent progress and perspectives,” in *Proc. 4th Berkeley Symp. Energy Efficient Electron. Syst. (E S)*, Oct. 2015, p. 1.

[29] T. Nozaki *et al.*, “Highly efficient voltage control of spin and enhanced interfacial perpendicular magnetic anisotropy in iridium-doped Fe/MgO magnetic tunnel junctions,” *NPG Asia Mater.*, vol. 9, no. 12, p. e451, Dec. 2017.

[30] M. Yi, H. Zhang, and B.-X. Xu, “Voltage-driven charge-mediated fast 180 degree magnetization switching in nanoheterostructure at room temperature,” *NPJ Comput. Mater.*, vol. 3, no. 1, p. 38, Sep. 2017.

[31] S. Zhao *et al.*, “Ionic liquid gating control of spin reorientation transition and switching of perpendicular magnetic anisotropy,” *Adv. Mater.*, vol. 30, no. 30, Jul. 2018, Art. no. 1801639.

[32] U. Bauer, M. Przybylski, and G. S. D. Beach, “Voltage control of magnetic anisotropy in Fe films with quantum well states,” *Phys. Rev. B, Condens. Matter*, vol. 89, May 2014, Art. no. 174402, doi: 10.1103/PhysRevB.89.174402.

[33] Q. Yang *et al.*, “Voltage control of perpendicular magnetic anisotropy in multiferroic $(Co/Pt)_3/PbMg_{1/3}Nb_{2/3}O_3$-$PbTiO_3$ heterostructures,” *Phys. Rev. A, Gen. Phys.*, vol. 8, no. 4, Oct. 2017, Art. no. 044006, doi: 10.1103/PhysRevApplied.8.044006.

[34] T. Nozaki *et al.*, “Enhancement in the interfacial perpendicular magnetic anisotropy and the voltage-controlled magnetic anisotropy by heavy metal doping at the Fe/MgO interface,” *APL Mater.*, vol. 6, no. 2, Feb. 2018, Art. no. 026101.

[35] J. Suwardy, M. Goto, Y. Suzuki, and S. Miwa, “Voltage-controlled magnetic anisotropy and Dzyaloshinskii–Moriya interactions in CoNi/MgO and CoNi/Pd/MgO,” *Jpn. J. Appl. Phys.*, vol. 58, no. 6, Jun. 2019, Art. no. 060917.

[36] Q. Yang *et al.*, “Ionic liquid gating control of RKKY interaction in FeCoB/Ru/FeCoB and $(Pt/Co)_2/Ru/(Co/Pt)_2$ multilayers,” *Nature Commun.*, vol. 9, no. 1, p. 991, Mar. 2018.

[37] A. O. Leon, J. d’Albuquerque e Castro, J. C. Retamal, A. B. Cahaya, and D. Altbir, “Manipulation of the RKKY exchange by voltages,” *Phys. Rev. B, Condens. Matter*, vol. 100, no. 1, Jul. 2019, Art. no. 014403.

[38] M. Fechner, P. Zahn, S. Ostanin, M. Bibes, and I. Mertig, “Switching magnetization by 180° with an electric field,” *Phys. Rev. Lett.*, vol. 108, May 2012, Art. no. 197206, doi: 10.1103/PhysRevLett.108.197206.

[39] C.-Y. You and S. D. Bader, “Prediction of switching/rotation of the magnetization direction with applied voltage in a controllable interlayer exchange coupled system,” *J. Magn. Magn. Mater.*, vol. 195, no. 2, pp. 488–500, May 1999.

[40] M. A. Ruderman and C. Kittel, “Indirect exchange coupling of nuclear magnetic moments by conduction electrons,” *Phys. Rev.*, vol. 96, no. 1, pp. 99–102, Oct. 1954.

[41] T. Kasuya, “A theory of metallic ferro- and antiferromagnetism on Zener’s model,” *Prog. Theor. Phys.*, vol. 16, no. 1, pp. 45–57, Jul. 1956.

[42] K. Yosida, “Magnetic properties of Cu-Mn alloys,” *Phys. Rev.*, vol. 106, no. 5, pp. 893–898, Jun. 1957.

[43] S. S. P. Parkin and D. Mauri, “Spin engineering: Direct determination of the Ruderman-Kittel-Kasuya-Yosida far-field range function in ruthenium,” *Phys. Rev. B, Condens. Matter*, vol. 44, no. 13, pp. 7131–7134, Oct. 1991.

[44] R. Hao, L. Wang, and T. Min, “A novel STT-MRAM design with electric-field-assisted synthetic anti-ferromagnetic free layer,” *IEEE Trans. Magn.*, vol. 55, no. 3, pp. 1–6, Mar. 2019.

[45] M. J. Donahue and D. G. Porter, “OOMMF user’s guide, version 1.0,” Nat. Inst. Standards Technol., Gaithersburg, MD, USA, Tech. Rep. NISTIR 6376, 1999.

[46] A. V. Khvalkovskiy *et al.*, “High domain wall velocities due to spin currents perpendicular to the plane,” *Phys. Rev. Lett.*, vol. 102, no. 6, Feb. 2009, Art. no. 067206.

[47] T. L. Gilbert, “A Lagrangian formulation of the gyromagnetic equation of the magnetization field,” *Phys. Rev.*, vol. 100, p. 1243, Jan. 1955.

[48] L. D. Landau and E. Lifshitz, “On the theory of the dispersion of magnetic permeability in ferromagnetic bodies,” *Phys. Zeitsch. Sow.*, vol. 8, p. 153, Jun. 1935.

[49] J. Xiao, A. Zangwill, and M. D. Stiles, “Boltzmann test of Slonczewski’s theory of spin-transfer torque,” *Phys. Rev. B, Condens. Matter*, vol. 70, Nov. 2004, Art. no. 172405.

[50] X. Liu, W. Zhang, M. J. Carter, and G. Xiao, “Ferromagnetic resonance and damping properties of CoFeB thin films as free layers in MgO-based magnetic tunnel junctions,” *J. Appl. Phys.*, vol. 110, no. 3, Aug. 2011, Art. no. 033910.

[51] T. Devolder *et al.*, “Damping of $Co_xFe_{80-x}B_{20}$ ultrathin films with perpendicular magnetic anisotropy,” *Appl. Phys. Lett.*, vol. 102, no. 2, Jan. 2013, Art. no. 022407.

[52] S. Ikeda *et al.*, “A perpendicular-anisotropy CoFeB-MgO magnetic tunnel junction,” *Nature Mater.*, vol. 9, no. 9, pp. 721–724, Jul. 2010.

[53] S.-C. Oh *et al.*, “Bias-voltage dependence of perpendicular spin transfer torque in asymmetric MgO-based magnetic tunnel junctions,” in *Proc. APS Meeting Abstr.*, Mar. 2010, Art. no. L37.010. [Online]. Available: http://www.meetings.aps.org/Meeting/MAR10/Event/119978

[54] J. C. Sankey, Y.-T. Cui, J. Z. Sun, J. C. Slonczewski, R. A. Buhrman, and D. C. Ralph, “Measurement of the spin-transfer-torque vector in magnetic tunnel junctions,” *Nature Phys.*, vol. 4, no. 1, pp. 67–71, Jan. 2008.

[55] H. Kubota *et al.*, “Quantitative measurement of voltage dependence of spin-transfer torque in MgO-based magnetic tunnel junctions,” *Nature Phys.*, vol. 4, no. 1, pp. 37–41, Jan. 2008.

[56] A. M. Deac *et al.*, “Bias-driven high-power microwave emission from MgO-based tunnel magnetoresistance devices,” *Nature Phys.*, vol. 4, no. 10, pp. 803–809, Oct. 2008.

[57] D. V. Berkov, C. T. Boone, and I. N. Krivorotov, “Micromagnetic simulations of magnetization dynamics in a nanowire induced by a spin-polarized current injected via a point contact,” *Phys. Rev. B, Condens. Matter*, vol. 83, Feb. 2011, Art. no. 054420.

[58] M. Wyss *et al.*, “Imaging magnetic vortex configurations in ferromagnetic nanotubes,” *Phys. Rev. B, Condens. Matter*, vol. 96, no. 2, Jul. 2017, Art. no. 024423, doi: 10.1103/PhysRevB.96.024423.

[59] A. van den Brink *et al.*, “Spin-Hall-assisted magnetic random access memory,” *Appl. Phys. Lett.*, vol. 104, no. 1, Jan. 2014, Art. no. 012403.

[60] S. Ikeda *et al.*, “Magnetic tunnel junctions for spintronic memories and beyond,” *IEEE Trans. Electron Devices*, vol. 54, no. 5, pp. 991–1002, May 2007.

[61] R. Heindl, A. Chaudhry, and S. E. Russek, “Estimation of thermal stability factor and intrinsic switching current from switching distributions in spin-transfer-torque devices with out-of-plane magnetic anisotropy,” *AIP Adv.*, vol. 8, no. 1, Jan. 2018, Art. no. 015011, doi: 10.1063/1.5002139.

[62] S. Bhatti, R. Sbiaa, A. Hirohata, H. Ohno, S. Fukami, and S. N. Piramanayagam, “Spintronics based random access memory: A review,” *Mater. Today*, vol. 20, no. 9, pp. 530–548, Nov. 2017.

[63] S. Peng *et al.*, “Interfacial perpendicular magnetic anisotropy in sub-20 nm tunnel junctions for large-capacity spin-transfer torque magnetic random-access memory,” *IEEE Magn. Lett.*, vol. 8, pp. 1–5, 2017.

[64] N. Bukar, S. S. Zhao, D. M. Charbonneau, J. N. Pelletier, and J.-F. Masson, “Influence of the Debye length on the interaction of a small molecule-modified Au nanoparticle with a surface-bound bioreceptor,” *Chem. Commun.*, vol. 50, pp. 4947–4950, 2014.

[65] J. J. Kan *et al.*, “Systematic validation of 2x nm diameter perpendicular MTJ arrays and MgO barrier for sub-10 nm embedded STT-MRAM with practically unlimited endurance,” in *IEDM Tech. Dig.*, Dec. 2016, p. 27.

[66] C. Park *et al.*, “Low RA magnetic tunnel junction arrays in conjunction with low switching current and high breakdown voltage for STT-MRAM at 10 nm and beyond,” in *Proc. IEEE Symp. VLSI Technol.*, Jun. 2018, pp. 185–186.

[67] G. Jan *et al.*, “Demonstration of ultra-low voltage and ultra low power STT-MRAM designed for compatibility with 0x node embedded LLC applications,” in *Proc. IEEE Symp. VLSI Technol.*, Jun. 2018, pp. 65–66.

Authorized licensed use limited to: Xian Jiaotong University. Downloaded on August 05,2021 at 01:44:58 UTC from IEEE Xplore. Restrictions apply.